Biochimica et Biophysica Acta 1838 (2014) 237–243

Contents lists available at ScienceDirect

Biochimica et Biophysica Acta

journal homepage: www.elsevier.com/locate/bbamem

The projection structure of Kch, a putative potassium channel in *Escherichia coli*, by electron crystallography

Qie Kuang *, Pasi Purhonen, Caroline Jegerschöld, Hans Hebert **

Karolinska Institutet, Dept of Biosciences and Nutrition and KTH Royal Institute of Technology, School of Technology and Health, Novum, S-14183 Huddinge, Sweden

ARTICLE INFO

Article history:
Received 30 June 2013
Received in revised form 7 September 2013
Accepted 10 September 2013
Available online 19 September 2013

Keywords:
Electron microscopy
Projection map
Potassium channel
RCK
Membrane protein

ABSTRACT

The *kch* gene, the only potassium channel gene in *Escherichia coli*, has the property to express both full-length Kch and its cytosolic domain (RCK) due to a methionine at position 240. The RCK domains are believed to form an octameric ring structure and regulate the gating of the potassium channels after having bound certain ligands. Several different gating ring structures have been reported for the soluble RCK domains, however, these were studied isolated from their transmembrane parts. We previously reported an octameric structure of Kch in solution by electron microscopy and single particle reconstruction, composed of two tetrameric full-length proteins through RCK interaction. To exclude the effect of the detergent, we have now performed an electron crystallographic study of the full-length Kch in membrane bound form. Well-ordered two-dimensional crystals were grown in a natural phospholipid environment. A projection map merged from the fifteen best images extended to 6 Å resolution. The *c*12 two-sided plane group of the two-dimensional crystals showed that Kch crystallized as two symmetrically related overlapping layers. The arrangement suggests that the two layers of RCK domains are shifted with respect to each other and the RCK octameric gating ring of Kch does not form under the crystallization condition.

1. Introduction

Potassium channels play vital roles in cellular processes, for example in transfer of electrical signals in excitable nerve and muscle cells. They exist in virtually all living organisms, except for some parasites and inner organelles such as mitochondria and chloroplasts [1]. Only one putative potassium channel, Kch, is reported to exist in *Escherichia coli* (*E. coli*) [2]. Kch has a conserved signature sequence, TVGYG, as in other highly potassium ion selective channels. Besides its six transmembrane helices (6-TM, S1–S6), it has a large cytosolic domain, referred to as the regulator of the conductance of potassium ion (RCK) [3]. The RCK domain is believed to act as a receptor for binding of various ligands usually at the C-terminus, and is present in various prokaryotic cells [1]. As in MthK (a calcium gated potassium channel from *Methanobacterium thermoautotrophicum*) [4,5], the *kch* gene has an internal start codon for expression of RCK. Four Kch and four RCK molecules are proposed to assemble to form an octameric gating ring in vivo [4]. Although the RCK structure from Kch has been solved (PDB: 1ID1) [3], the function and regulation of Kch are not yet completely understood [1,6,7].

Since the structure of KcsA (a potassium channel from *Streptomyces lividans*) was determined by X-ray crystallography [8], tremendous progress has been made in understanding the mechanism of potassium channels. Among these, the structure of Kv1.2 (a voltage gated potassium channel from *Rattus norvegicus*) illustrates an open conformation [9–11] and the structure of MlotiK1 (a non-voltage gated, but cyclic nucleotide regulated potassium channel from *Mesorhizobium loti*) represents a closed conformation [12]. Both Kv1.2 and MlotiK1 have 6-TM, where the last two helices (S5–S6) constitute a pore-forming domain to conduct potassium ions. One major difference between these two channels is that the former has arginine residues at every third position in the fourth helix (S4) which are absent in the latter [9–12]. These arginine residues are believed to sense the alteration in the membrane electric field and lead to the conformational changes of the channel [10]. However, the function of the sensor domains (the first to the fourth helix, S1–S4) lacking these arginine residues is not understood in the non-voltage gated potassium channels. Similar to MlotiK1, Kch also lacks a conventional sequence pattern of arginine residues in S4 [2].

Although the structures of the potassium channels solved by X-ray crystallography give us invaluable information, the majority of them are crystallized in the presence of detergent that may influence their structures. For example, the voltage sensor domain of KvAP (a voltage gated potassium channel from *Aeropyrum pernix*) is believed to be in a non-native conformation due to the lack of constraints from the planar lipid membrane [13,14]. In order to study Kch in a more natural

* Corresponding author. Tel.: +46 8 524 81072, +46 76 2123639; fax: +46 8 524 81 135.
** Corresponding author. Tel.: +46 8 524 81 093, +46 73 358 62 24; fax: +46 8 524 81 135.
E-mail addresses: Qie.Kuang@ki.se (Q. Kuang), Hans.Hebert@ki.se (H. Hebert).

0005-2736/$ – see front matter © 2013 Elsevier B.V. All rights reserved.
http://dx.doi.org/10.1016/j.bbamem.2013.09.006

phospholipid environment, we have performed a structural study from two-dimensional (2D) crystals in the presence of 1,2-dioleoyl-sn-glycero-3-phosphocholine (DOPC). Here we report a merged projection map that extends to 6 Å resolution. In contrast to our previous single particle work from detergent solubilized specimens, which suggests that Kch forms a dimer of tetramer structure through RCK interaction [15], our present result suggests that the RCK octameric gating ring does not form under our crystallization condition.

2. Materials and methods

2.1. Construction of the Kch and KchM240L plasmids

The native *kch* gene from *E. coli* DH5α chromosomal DNA with a six-histidine-tag at the C-terminus was amplified by polymerase chain reaction. After digestion by NdeI (5′ end) and HindIII (3′ end) restriction enzymes, the *kch* gene was ligated with the pSP19T7LT vector [16] using T4 DNA ligase enzyme (Invitrogen) to construct the Kch plasmid.

Since the *kch* gene encodes both Kch and RCK proteins, we replaced the internal methionine codon at position 240 with leucine to prevent the expression of RCK. The construction of the KchM240L mutant plasmid was made according to the manufacturer's instructions (Stratagene).

2.2. Purification, negative staining and electron microscopy

The wild type (Kch) and mutant (KchM240L) proteins were expressed and purified as described in [15], with the following modifications: 1) Expression was performed in C43(DE3) strain (Lucigen) and the large scale expression was started from a 1:100 dilution; 2) The cell lysate was sonicated by ten times 30-second sonication pulses from an ultrasonic cell disruptor (Branson Sonifier 250) at 30% power and 30% duty cycle; and 3) All the purification buffers contained 150 mM KCl and 1 mM reduced glutathione (Sigma) together with *n*-dodecyl-β-D-maltopyranoside (DDM). After size exclusion chromatography (size exclusion column: Superdex200, Hiload 16/60, GE Healthcare), KchM240L sample was analyzed with negative stained electron microscopy as described previously [15]. The class averaged projection images were generated using EMAN2 [17].

2.3. Electron crystallographic study

The expression and purification procedure of KchM240L for 2D crystallization trials was similar to the one described ahead, with the following modifications: 1) The cells were cultured for another 4 h at 33 °C after induction with 1 mM isopropyl-β-D-thiogalactopyranoside (IPTG, Fermentas); and 2) The detergent was changed to Triton X-100. The membranes were solubilized with 4% Triton X-100 (Sigma) and the following purification buffers contained 0.1% reduced Triton X-100 (Sigma). The fractions of the size exclusion chromatography were pooled (approximately 10 ml) and concentrated (approximately 1 ml). This sample was verified by matrix assisted laser desorption ionization-time of flight mass spectrometry (MALDI-TOF MS) as described in [15]. The precursor fragments after MALDI-TOF MS was further ionized with a higher intensity and the generated product fragments were detected by a tandem MS. A lipid–detergent solution containing DOPC (Avanti) and 1% Triton X-100 (Roche) was mixed with the concentrated sample at a lipid-to-protein ratio at 0.2 (w/w). After incubation at room temperature for 30 min, the lipid–protein–detergent mixture was dialyzed with the following buffer: 20 mM Tris–HCl at pH 9, 20% glycerol, 100 mM KCl, 0.1 mM EDTA, 1 mM reduced glutathione and 100–200 mM $MgCl_2$ at 19 °C for one week.

Well-ordered 2D crystals were mixed with 7% trehalose (Sigma) on 400 mesh copper grids prepared by the back injection method [18] and subsequently transferred into a JEOL JEM-2100F electron microscope (Jeol). All the data collection taken at 50,000× magnification was performed at liquid nitrogen temperature (cryo-EM) with defocus values ranging from 0.5 μm to 1.5 μm. The images were recorded under low-dose conditions (~10 electrons per $Å^2$) on Kodak SO-163 electron image films (Electron Microscopy Sciences) at 200 kV accelerating voltage. Well-ordered areas (4000 × 4000 pixels) from the micrographs were scanned with a pixel size of 7 μm using a Zeiss SCAI scanner (Carl Zeiss). The MRC image processing suite [19] and the Ximdisp visualization tool [20] were used to process individual images, according to the procedure described in [21]. The defocus was determined by the CTFTILT program and further verified manually, and the CTFAPPLY program was used to adjust the contrast transfer function (CTF) effect. The best images were merged for calculation of the projection map. The *c*12 symmetry was determined using the ALLSPACE program [22]. The plot showing the completeness of reflections to 6 Å was made from 2dx_plotreska in 2dx [23,24]. Since both MlotiK1 and Kch have 6-TMs with no arginine residue in S4 [2,12] and both of them are from prokaryotes, the structure of the transmembrane part of MlotiK1 (PDB: 3BEH) was used as a model to match the KchM240L projection map. The protein sequences were initially aligned using ClustalW2 [25] and then modified manually by matching the observed structure of 6-TM, pore helix and the selectivity filters of MlotiK1 (PDB: 3BEH, the sequence is shown in SI Fig. 8 in [12]) with the predicted counterparts of Kch [2]. The *c*12 symmetrized projection map of MlotiK1 in unit cell dimensions as in the 2D crystals of KchM240L was generated using CCP4 [26–28]. The superimposition of the adapted MlotiK1 model and the KchM240L projection map was made using Chimera [29] and GNU Image Manipulation Program (GIMP). Two models were generated based on the two distinct density domains in the symmetrized projection map. The transmembrane part of MlotiK1 (PDB: 3BEH) was overlaid into either of them to maximize the overlapping of the assumed pore-forming domains, with the length of the square like pore-forming domain equal to 45 Å.

3. Results

3.1. Purification, negative staining and electron microscopy

In order to reduce the heterogeneity from RCK, which may influence the later 2D crystallization step, we constructed the KchM240L plasmid in which the internal methionine codon at position 240 was replaced by leucine. KchM240L has been reported to be functionally similar to the native Kch [6]. Since Kch has been expressed, purified and subjected to electron microscopy for single particle reconstruction previously [15], we expressed and purified C-terminally histidine tagged KchM240L in the same way as Kch to study whether there was any difference between these two proteins.

The expressed Kch or KchM240L proteins were first purified with immobilized metal affinity chromatography (IMAC) and followed by size exclusion chromatography. There was no significant difference of the oligomeric patterns between Kch (46 kDa) and KchM240L in either size exclusion chromatographs (Fig. 1A) or SDS-PAGE gel analysis (band ii in Fig. 1B and C). However, RCK (19 kDa, band i in Fig. 1B and C) was not detected when KchM240L was expressed (lanes 1 and 2 in Fig. 1B and C). The majority of RCK elutes in a broad volume range and some RCK remains bound to Kch after size exclusion chromatography of Kch (data not shown here, SDS-PAGE gel analysis was shown in Fig. 2A in Ref [15]).

Several other potassium channels were reported to have heterogeneity in their oligomeric patterns, which might reflect the different equilibria of oligomer–monomer of each channel [30,31]. The high molecular band (oligomer in band iii of Fig. 1B and C) converted to the low molecular band (monomer in band ii of Fig. 1B and C) with alkaline but not acid treatment (data now shown). Both of the two major bands (band iii and band ii in Fig. 1B and C) from KchM240L were verified to contain the RCK domain by matrix assisted laser desorption ionization-time of flight mass spectrometry (the verification of Kch was done in [15]). Furthermore, one trypsin digested fragment (size:

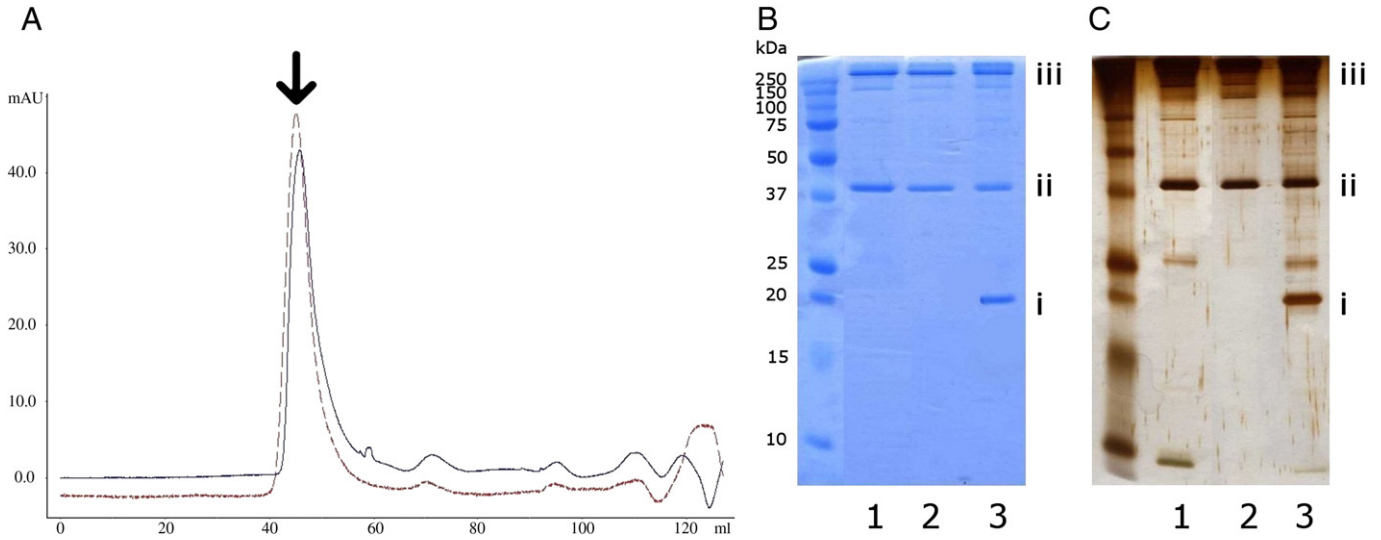

Fig. 1. Purification results of Kch and KchM240L in DDM. (A) Size exclusion chromatographs of Kch (red) and KchM240L (blue). The arrow indicates where the peak approximately elutes at 45 ml. (B and C) 15% homogeneous SDS-PAGE gel analysis with Coomassie (B) and silver stain (C). The Kch sample after IMAC loaded in lane 3 in both (B) and (C) shows three major bands: band iii, band ii and band i. The KchM240L sample after IMAC loaded in lane 1 in both (B) and (C) shows two major bands: band iii and band ii. The bands iii, ii and i indicate the assumed position of the oligomer, monomer and RCK, respectively. The purified KchM240L sample after size exclusion chromatography is loaded in lane 2 in both (B) and (C). The protein marker bands are shown close to lane 1.

1742 Da) was subjected to tandem mass spectrometry. The deduced amino acid sequence (VTVISNL) matches the theoretical peptide (GQNVTVISNLPEDDIK$^{266-281}$).

After size exclusion chromatography, the homogeneity state of KchM240L was analyzed by electron microscopy following negative staining. The class averaged projection images show that the particles were composed of three domains with the middle domains distinct from their top or bottom counterparts (Fig. 2), which is similar to the ones of Kch (Fig. 3B in [15]).

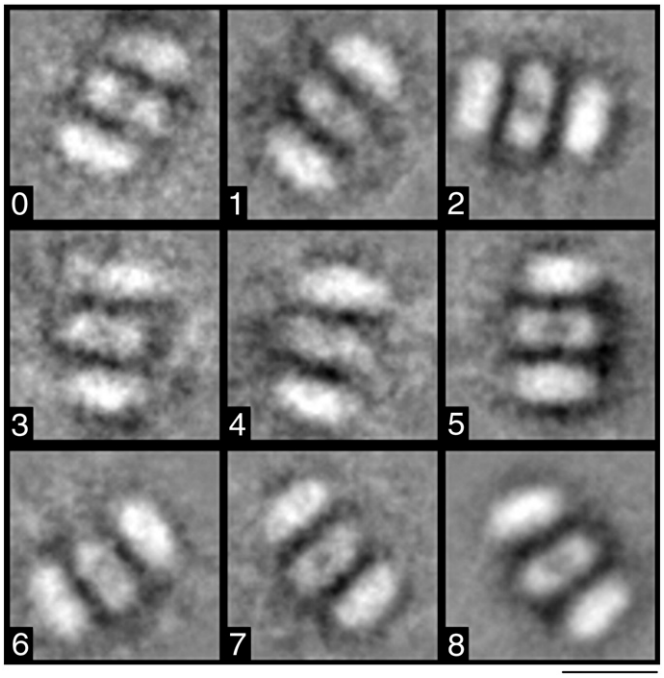

Fig. 2. The typical class averaged projection images of KchM240L sample purified in DDM after size exclusion chromatography. Samples were negatively stained with 1% uranyl acetate and the micrographs were taken at 60,000× magnification. Due to the rod shaped sample property, only the side view projection images are found in the micrographs and included. The class averaged projection images generated using a standard EMAN2 procedure show that the KchM240L single molecules are composed of three distinct domains. The middle domains which are different compared to the top or bottom domains are interpreted to arise from the RCK octameric gating ring as proposed in [15]. The black scale bar is 100 Å.

3.2. Electron crystallographic study

Previously, Kch was purified in DDM [15] and 2D crystallization trials did not succeed. Although KchM240L does not express soluble RCK (Fig. 1), which increases its homogeneity, no 2D crystal was obtained from the sample purified in DDM. However, the KchM240L sample purified in Triton X-100 did form crystals and the largest of them grew to about 1 μm (Fig. 3). Several lipids (1,2-dilauroyl-*sn*-glycero-3-phosphocholine (DLPC), 1,2-dimyristoyl-*sn*-glycero-3-phosphocholine (DMPC), 1,2-dioleoyl-sn-glycero-3-phosphocholine (DOPC), *E. coli* extract polar and liver L-α-phosphatidylcholine) were tested and crystals were formed most readily using DOPC (an eighteen carbon length unsaturated fatty acid). In the crystals, KchM240L protein units were arranged in a rectangular unit cell having dimension 144 Å × 84 Å with an included angle of 90° (Table 1). The

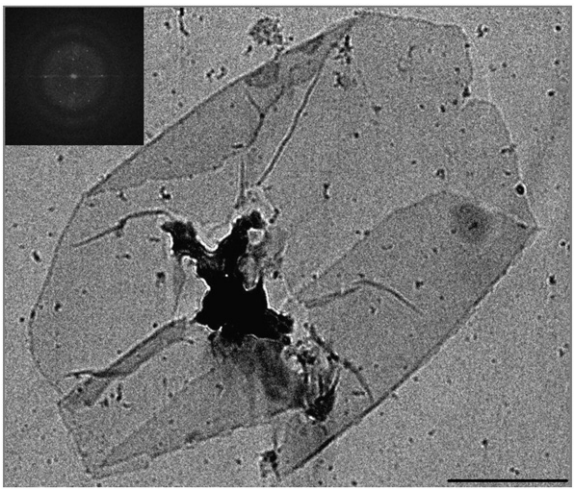

Fig. 3. An electron micrograph of a KchM240L 2D crystal embedded in 1% uranyl acetate. The computed Fourier transform of the crystalline area shows a single lattice on the inset. The scale bar is 0.25 μm.

Table 1
Electron crystallographic data.

Number of images	6	
Number of diffraction patterns	15	
Unit cell parameters	a = 144 ± 1.9 Å	
	b = 84 ± 1.0 Å	
	γ = 90 ± 0.5°	
Range of defocus (Å)	5000–15000	
Space group	*c*12	
Σ‖Ø(h, k)| − |Ø(h, −k)‖ / n, n number of comparisons	22.0°	
Resolution limit of 12 merged images	100–6 Å	
Total number of unique reflections	135	
Completeness to 6 Å, IQ ≤ 7	90.6%	
Overall merging phase residual to 6 Å, IQ ≤ 7	23.5°	
Merging phase residual (no. observations, IQ ≤ 4)	Resolution range (Å)	Angle (°)
	100–14	17 (544)
	14–10	23 (485)
	10–8	33 (303)
	8–6	42 (111)

computed Fourier transforms of images of crystalline areas from the frozen crystals often showed diffraction peaks that could be indexed on 2–3 independent but identical lattices (Fig. 4A). The stacked crystals were not superimposed in register since the lattices had various in-plane rotations with respect to each other. These lattices could be processed separately and each pattern could be treated as arising from a single lattice (Fig. 4B and C).

Amplitudes and phases of 126 spots could be measured from the merged data out of a total of 139 possible ones in the projected asymmetric unit at 6 Å resolution (Fig. 5). A *c*12 symmetry plane group was assigned based on Fourier component relationships using the ALLSPACE program [22] (Supplementary Fig. S1). The symmetry was also inspected manually by observing the relationship of the projection densities in the unsymmetrized merged map (Fig. 6A) and to what extent the phases of the structure factors were satisfying the phase relationships, Ø(h, k) = −Ø(h, −k), following origin refinement (Table 1). A temperature factor of $B = -300$ Å^2 was applied when calculating the final merged projection map to boost the fall-off of the amplitudes at intermediate and high resolution (Fig. 6B). The two-fold rotation and two-fold screw symmetry elements were parallel to the b-axis. No symmetry element was found along the a-axis. The domain outlined in the square region (Fig. 6B) is mirrored by a two-fold rotation symmetry element while the other high density domains outlined in the circle regions (Fig. 6B) are rotated 180° along the b-axis direction and translated by a half unit cell length relatively to each other. Interestingly, no crystallographic four-fold symmetry element was found as expected from the other published potassium channel structures studied by X-ray crystallography.

4. Discussion

4.1. A dimer of tetramer arrangement in detergent solution

Kch is a putative ligand-gated potassium channel with its RCK domain homologous to MthK and BKca (a large conductance potassium channel, both voltage and calcium gated, from *Homo sapiens*) [3,4]. Although the ligand of Kch has not been identified, RCK also in Kch has a tendency to form dimers, either with another soluble RCK as in the

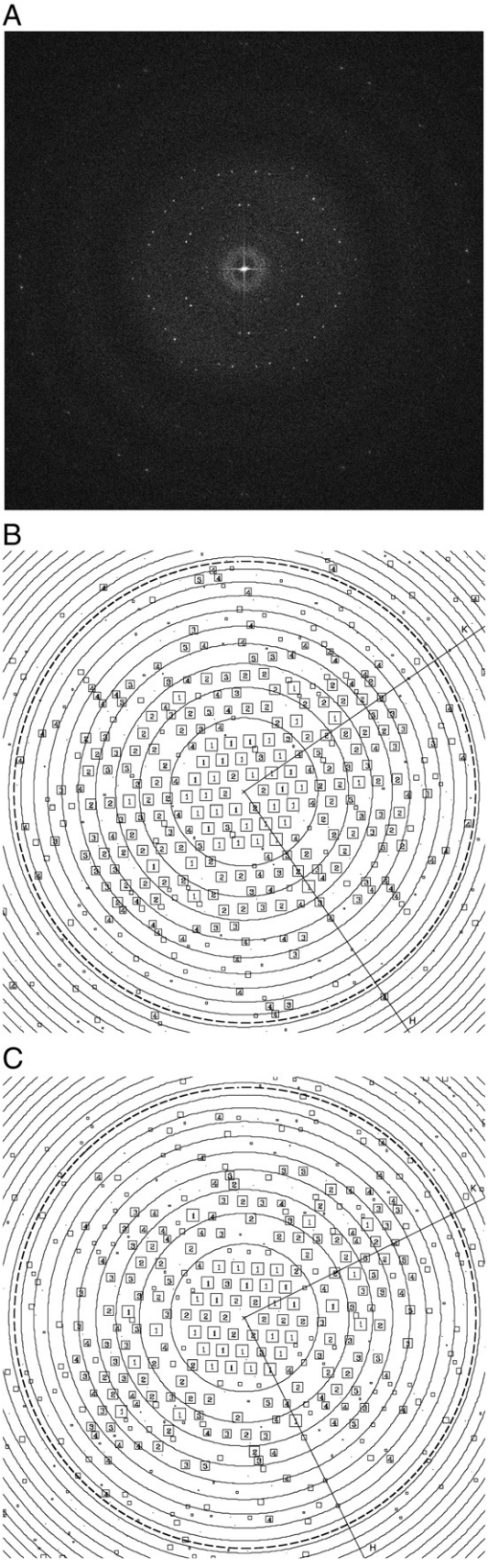

Fig. 4. Computed Fourier transform amplitudes of a cryo-EM image of a 2D crystal of KchM240L. (A) The crystal embedded in trehalose and frozen in liquid nitrogen shows two lattices in the computed Fourier transform. (B) and (C) show two different indexing of the Fourier transform after unbending. The lattices in (B) and (C) could be processed separately. The IQ value representing the signal to noise ratio is shown with different sizes of boxes and numbers. Stronger spots have lower IQ values. The spots with IQ ≤ 4 are shown in the boxes by their numbers and the spots with IQ > 4 are shown with decreased box sizes. The circle of dashes depicts the 6 Å resolution limit. The concentric circles represent the zero crossings of the contrast transfer function (CTF). The lattice vectors are indicated by H and K. For lattice in (B), the phase residual determined after ALLSPACE [22] of *c*12 symmetry is 27.0° (90° random) and the overall phase residual determined by ORIGTILTK after application of *c*12 symmetry is 19.7°. The result of ALLSPACE is shown in Supplementary Fig. S1.

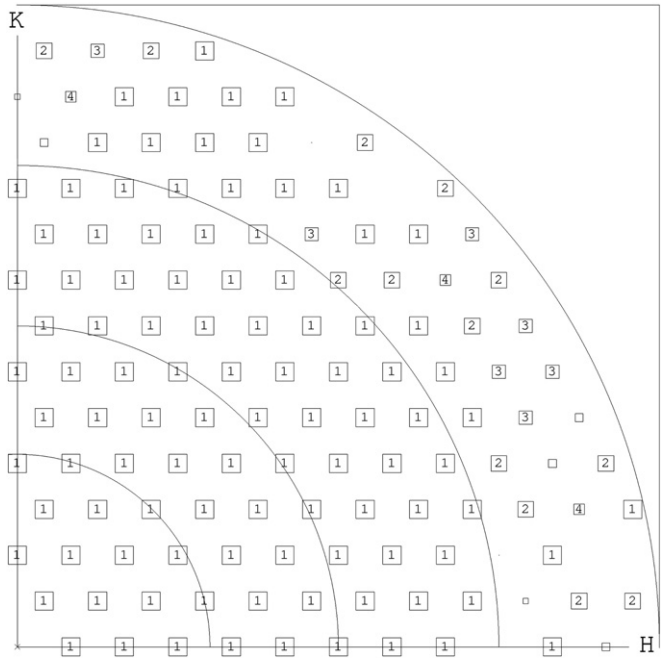

Fig. 5. The completeness plot. It shows the lattice unbending improved, contrast transfer function (CTF) corrected, merged and symmetry applied spots distribution to 6 Å resolution. The symbols indicate the figure of merit (FOM) of each reflection. The decreasing quality of FOM is represented by the increasing numbers in the symbols with smaller boxes: the value of FOM >95, >90, >85, >80, >75, >70, >65, >60, and <60 is calculated as the symbol 1, 2, 3, 4, 5, 6, 7, 8, and 9, respectively. Only the symbols <5 are shown in box with numbers. The lattice vectors are indicated by H and K. The concentric rings correspond to the 20, 12, 8 and 6 Å resolution, respectively.

crystal structure shown by [3] or with the RCK domain of a full-length Kch subunit suggested in [15]. In the latter, a single particle reconstruction based on electron microscopy images of detergent solubilized and negatively stained Kch showed that Kch had a dimer of tetramer arrangement in solution [15]. Considering the functional identity of Kch and KchM240L [6] and similar class averaged projection images of them (Fig. 2), we expect that KchM240L in detergent solution is likely to adopt a dimer of tetramer arrangement in solution. However, the present electron crystallographic study in which the proteins are embedded in a more natural phospholipid environment suggests a different assembly of KchM240L.

4.2. Two symmetrically related overlapping layers

From the merged projection map it was clear that neither crystallographic nor local four-fold symmetry perpendicular to the plane of the membrane, as would have been expected for a potassium channel, was present in the 2D crystals obtained under our crystallization conditions (Fig. 6A). We interpret this symmetry reduction as primarily arising from projections of two or more overlapping layers of protein and lipid with the protein molecules in adjacent layers having different in-plane rotations and/or different positions relatively to the unit cell. The symmetrized projection map showed two distinct density domains, which are outlined in a square and two circles in Fig. 6B. The two-fold rotation along the b-axis of the *c*12 two-sided plane group is centered on a high density zone in the square region. Thus, this symmetry axis as well as the two-fold screw axis is located in between two layers and the crystals can be described as consisting of two identical, symmetry related layers. From preliminary tilting experiments (data not shown) and the discussion in the Supplementary text with accompanying Supplementary figures, the arrangement of a dimer of tetramer and the option of assembling more than two layers could be discarded.

Based on the symmetrized projection map (Fig. 6B) we generated a packing model of the channel domain using the structurally similar transmembrane part of MlotiK1 (PDB: 3BEH, the sequence alignment is shown in Supplementary Fig. S2) as depicted in Fig. 6C and Supplementary Fig. S3. The pore-forming domains (S5–S6) were centered on the circle regions having maximum overlapping density and the sensor domains (S1–S4) were on the square regions. This positioning and rotation together with the symmetry elements of the 2D crystals result in an arrangement of the protein with minimum steric hindrance. It follows from these assignments that two adjacent KchM240L molecules from the two membrane layers are laterally shifted relatively to each other. Thus, this model is not compatible with the formation of dimers of KchM240L tetramers generated by an octameric ring arrangement of RCK. From the projection map it is not possible to conclude if the protein molecules in the two layers are oriented with their intra- or extracellular protrusions towards the interface between the two layers.

The densities from the adapted model and the projection map do not correspond perfectly. Most importantly, the matching was concentrated to the transmembrane region using MlotiK1, which is lacking an RCK domain. Thus, additional density is expected from the expansion with these soluble domains. This could account for some of the density in the projection map that doesn't have overlapping atoms from the matched protein (Fig. 6C and Supplementary Fig. S3A). We believe the free RCK monomers form an RCK dimer with its partner from the adjacent subunits, since the dimer interface formed by the helix–strand–helix (αF–βG–αG) is hydrophobic, well packed and buries an extensive area when inserting to each other [3]. On the other hand there are also areas of the square region in Fig. 6B lacking projection map density where the matched proteins display parts of their sensor domains. This suggests that the sensor domains are exposed to forces in the 2D crystal environment that induce deviations from a local four-fold symmetry. High mobility of the sensor domains has been observed [10–14] and different orientations within the lipid bilayers may be due to the lipid–lipid, lipid–sensor or sensor–sensor interactions. Interestingly, our observation is in accordance with the previous electron crystallographic study of MlotiK1, in which the electron density from the sensor is much weaker compared to the one from pore-forming domain [32]. The authors have tested three possibilities and proposed that this discrepancy is due to the high mobility or multiple orientation of the sensor relative to the pore-forming domain [32].

Currently, we don't know whether this shifted RCK arrangement has any physiological role in *E. coli*. Four free soluble RCK may [4] or may not [6] form an octameric gating ring with four Kch in situ. Our result suggests that RCK does not form an octameric gating ring and it probably only retains the dimer arrangements under our crystallization condition.

5. Conclusion

Our previous single particle reconstruction of Kch, the putative potassium channel in *E. coli*, showed that it forms a dimer of tetramer structure in solution [15]. To determine the effect of lipid environment for this membrane protein, we performed an electron crystallographic study. Well-ordered 2D crystals showed information to 6 Å resolution. A shifted two layer assembly is suggested from overlaying a model on the merged projection map.

Supplementary data to this article can be found online at http://dx.doi.org/10.1016/j.bbamem.2013.09.006.

Acknowledgements

We thank Professor Serhiy Souchelnytskyi for the guidance of the mass spectrometry verification experiment. We also thank Drs. Wu Shangrung, Harriet Nilsson, and Philip Koeck for their comments of this manuscript. This work was supported by the Swedish Research Council and the Karolinska Institutet Center for Biosciences.

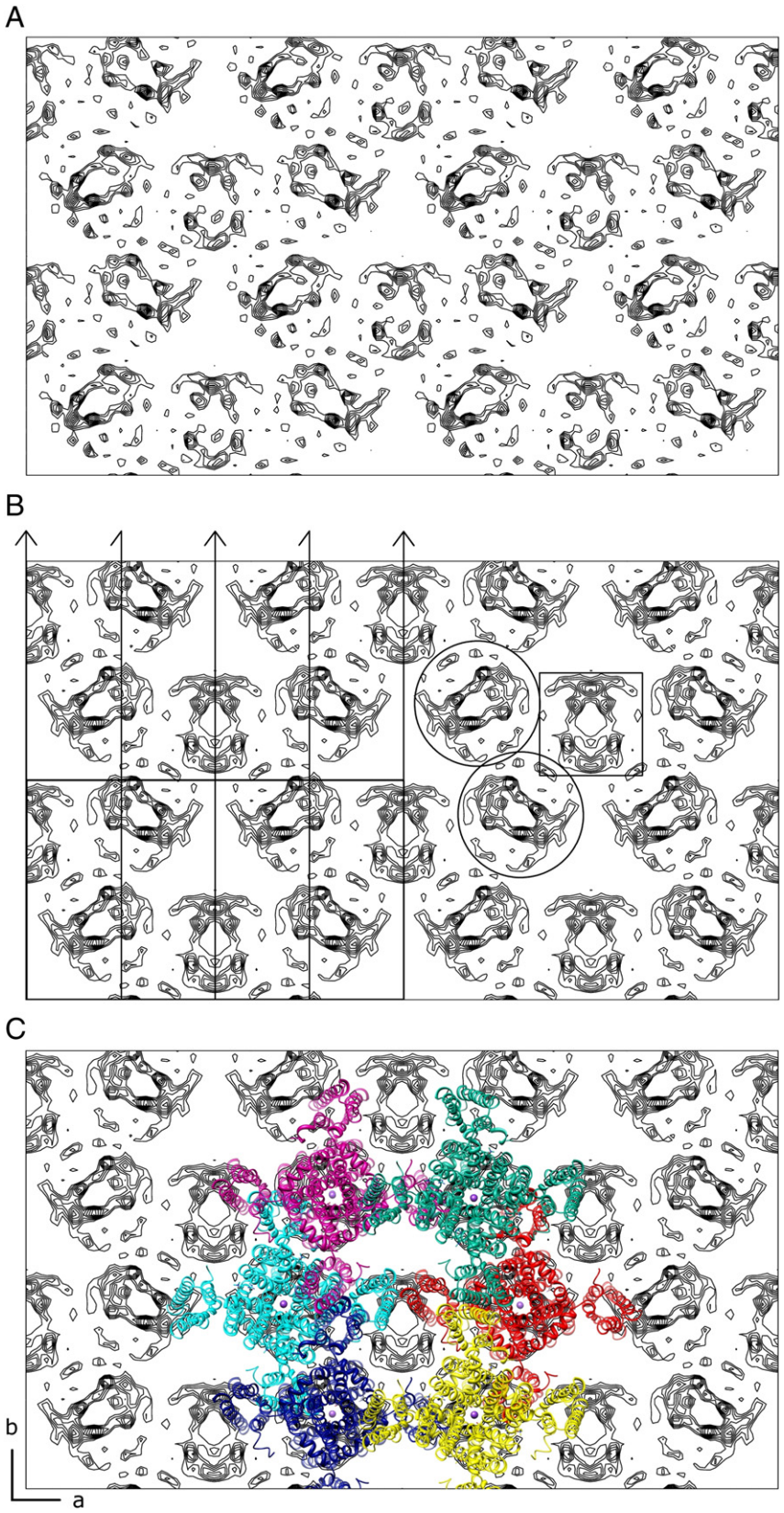

Fig. 6. A 2 × 2 unit cell projection contour plot map and the proposed superimposition model. A temperature factor of $B = -300$ Å^2 was applied to both unsymmetrized map (A) and symmetrized map (B). In (B), one unit cell is outlined in a box. Along the b-axis, full arrows indicate the two-fold rotation and the half arrows indicate the two-fold screw symmetry elements. Three different regions are outlined in a square and two circles. (C) The overlaying model of KchM240L in a shifted layer arrangement. The structure of the transmembrane part of MlotiK1 (PDB: 3BEH) is used to represent the corresponding sensor and pore-forming domains of KchM240L. The MlotiK1 ribbon presentation fits the projection map while keeping its original size. The tetramers in red, magenta and blue are in the top layer and those in cyan, green and yellow are in the bottom layer. The two layers of RCK domains are shifted relatively to each other and not modeled due to their uncertain positions. The directions of the unit cell vectors a (= 144 Å) and b (= 84 Å) are labeled. The positive contours shown as continuous lines indicate the peaks of density above the average. The corresponding projection map of (C), with the MlotiK1 density distribution shown, is presented in Supplementary Fig. S3A and the map from the ones without the sensor domains is presented in Supplementary Fig. S3B.

References

[1] M.M. Kuo, W.J. Haynes, S.H. Loukin, C. Kung, Y. Saimi, Prokaryotic K(+) channels: from crystal structures to diversity, FEMS Microbiol. Rev. 29 (2005) 961–985.
[2] R. Milkman, An *Escherichia coli* homologue of eukaryotic potassium channel proteins, Proc. Natl. Acad. Sci. U. S. A. 91 (1994) 3510–3514.
[3] Y. Jiang, A. Pico, M. Cadene, B.T. Chait, R. MacKinnon, Structure of the RCK domain from the *E. coli* K^+ channel and demonstration of its presence in the human BK channel, Neuron 29 (2001) 593–601.
[4] Y. Jiang, A. Lee, J. Chen, M. Cadene, B.T. Chait, R. MacKinnon, Crystal structure and mechanism of a calcium-gated potassium channel, Nature 417 (2002) 515–522.
[5] V.P. Pau, F.J. Smith, A.B. Taylor, L.V. Parfenova, E. Samakai, M.M. Callaghan, K. Abarca-Heidemann, P.J. Hart, B.S. Rothberg, Structure and function of multiple Ca^{2+}-binding sites in a K^+ channel regulator of K^+ conductance (RCK) domain, Proc. Natl. Acad. Sci. U. S. A. 108 (2011) 17684–17689.
[6] M.M. Kuo, Y. Saimi, C. Kung, Gain-of-function mutations indicate that *Escherichia coli* Kch forms a functional K^+ conduit in vivo, EMBO J. 22 (2003) 4049–4058.
[7] W. Epstein, The roles and regulation of potassium in bacteria, Prog. Nucleic Acid Res. Mol. Biol. 75 (2003) 293–320.
[8] D.A. Doyle, J. Morais Cabral, R.A. Pfuetzner, A. Kuo, J.M. Gulbis, S.L. Cohen, B.T. Chait, R. MacKinnon, The structure of the potassium channel: molecular basis of K^+ conduction and selectivity, Science 280 (1998) 69–77.
[9] S.B. Long, E.B. Campbell, R. Mackinnon, Crystal structure of a mammalian voltage-dependent Shaker family K^+ channel, Science 309 (2005) 897–903.
[10] S.B. Long, E.B. Campbell, R. Mackinnon, Voltage sensor of Kv1.2: structural basis of electromechanical coupling, Science 309 (2005) 903–908.
[11] S.B. Long, X. Tao, E.B. Campbell, R. MacKinnon, Atomic structure of a voltage-dependent K^+ channel in a lipid membrane-like environment, Nature 450 (2007) 376–382.
[12] G.M. Clayton, S. Altieri, L. Heginbotham, V.M. Unger, J.H. Morais-Cabral, Structure of the transmembrane regions of a bacterial cyclic nucleotide-regulated channel, Proc. Natl. Acad. Sci. U. S. A. 105 (2008) 1511–1515.
[13] Y. Jiang, A. Lee, J. Chen, V. Ruta, M. Cadene, B.T. Chait, R. MacKinnon, X-ray structure of a voltage-dependent K^+ channel, Nature 423 (2003) 33–41.
[14] S.Y. Lee, A. Lee, J. Chen, R. MacKinnon, Structure of the KvAP voltage-dependent K^+ channel and its dependence on the lipid membrane, Proc. Natl. Acad. Sci. U. S. A. 102 (2005) 15441–15446.
[15] A.K. Lundback, S.A. Muller, A. Engel, H. Hebert, Assembly of Kch, a putative potassium channel from *Escherichia coli*, J. Struct. Biol. 168 (2009) 288–293.
[16] R. Weinander, E. Mosialou, J. DeJong, C.P. Tu, J. Dypbukt, T. Bergman, H.J. Barnes, J.O. Hoog, R. Morgenstern, Heterologous expression of rat liver microsomal glutathione transferase in simian COS cells and *Escherichia coli*, Biochem. J. 311 (Pt 3) (1995) 861–866.
[17] G. Tang, L. Peng, P.R. Baldwin, D.S. Mann, W. Jiang, I. Rees, S.J. Ludtke, EMAN2: an extensible image processing suite for electron microscopy, J. Struct. Biol. 157 (2007) 38–46.
[18] D.N. Wang, W. Kuhlbrandt, High-resolution electron crystallography of light-harvesting chlorophyll a/b-protein complex in three different media, J. Mol. Biol. 217 (1991) 691–699.
[19] R.A. Crowther, R. Henderson, J.M. Smith, MRC image processing programs, J. Struct. Biol. 116 (1996) 9–16.
[20] J.M. Smith, Ximdisp — a visualization tool to aid structure determination from electron microscope images, J. Struct. Biol. 125 (1999) 223–228.
[21] M. Yeager, V.M. Unger, A.K. Mitra, Three-dimensional structure of membrane proteins determined by two-dimensional crystallization, electron cryomicroscopy, and image analysis, Methods Enzymol. 294 (1999) 135–180.
[22] J.M. Valpuesta, J.L. Carrascosa, R. Henderson, Analysis of electron microscope images and electron diffraction patterns of thin crystals of phi 29 connectors in ice, J. Mol. Biol. 240 (1994) 281–287.
[23] B. Gipson, X. Zeng, Z.Y. Zhang, H. Stahlberg, 2dx — user-friendly image processing for 2D crystals, J. Struct. Biol. 157 (2007) 64–72.
[24] B. Gipson, X. Zeng, H. Stahlberg, 2dx_merge: data management and merging for 2D crystal images, J. Struct. Biol. 160 (2007) 375–384.
[25] M.A. Larkin, G. Blackshields, N.P. Brown, R. Chenna, P.A. McGettigan, H. McWilliam, F. Valentin, I.M. Wallace, A. Wilm, R. Lopez, J.D. Thompson, T.J. Gibson, D.G. Higgins, Clustal W and Clustal X version 2.0, Bioinformatics 23 (2007) 2947–2948.
[26] R.J. Read, A.J. Schierbeek, A phased translation function, J. Appl. Crystallogr. 21 (1988) 490–495.
[27] M.D. Winn, C.C. Ballard, K.D. Cowtan, E.J. Dodson, P. Emsley, P.R. Evans, R.M. Keegan, E.B. Krissinel, A.G. Leslie, A. McCoy, S.J. McNicholas, G.N. Murshudov, N.S. Pannu, E.A. Potterton, H.R. Powell, R.J. Read, A. Vagin, K.S. Wilson, Overview of the CCP4 suite and current developments, Acta Crystallogr. D: Biol. Crystallogr. 67 (2011) 235–242.
[28] L. Ten, Efficient structure-factor calculation for large molecules by the fast Fourier transform, Acta Crystallogr. A 33 (1977) 486–492.
[29] E.F. Pettersen, T.D. Goddard, C.C. Huang, G.S. Couch, D.M. Greenblatt, E.C. Meng, T.E. Ferrin, UCSF Chimera — a visualization system for exploratory research and analysis, J. Comput. Chem. 25 (2004) 1605–1612.
[30] D.M. Cortes, E. Perozo, Structural dynamics of the Streptomyces lividans K^+ channel (SKC1): oligomeric stoichiometry and stability, Biochemistry 36 (1997) 10343–10352.
[31] L. Heginbotham, E. Odessey, C. Miller, Tetrameric stoichiometry of a prokaryotic K^+ channel, Biochemistry 36 (1997) 10335–10342.
[32] G.M. Clayton, S.G. Aller, J. Wang, V. Unger, J.H. Morais-Cabral, Combining electron crystallography and X-ray crystallography to study the MlotiK1 cyclic nucleotide-regulated potassium channel, J. Struct. Biol. 167 (2009) 220–226.